Computational and Structural Biotechnology Journal 21 (2023) 3796–3809

Contents lists available at ScienceDirect

Computational and Structural Biotechnology Journal

journal homepage: www.elsevier.com/locate/csbj

Research article

Characterizations of annexin A1-interacting proteins in apical membrane and cytosolic compartments of renal tubular epithelial cells

Paleerath Peerapen, Wanida Boonmark, Visith Thongboonkerd *

Medical Proteomics Unit, Research Department, Faculty of Medicine Siriraj Hospital, Mahidol University, Bangkok 10700, Thailand

ARTICLE INFO

Keywords:
Bioinformatics
Calcium
Immunoprecipitation
Kidney stone
Mass spectrometry
Oxalate
Proteomics

ABSTRACT

Annexin A1 (ANXA1) is a multifunctional calcium-binding protein that can bind to membrane phospholipids. Under high-calcium condition, ANXA1 expression increases on renal epithelial cell surface, leading to enhanced adhesion of calcium oxalate (CaOx) crystal (stone material) onto the cells. To regulate various cellular processes, ANXA1 interacts with many other intracellular protein partners. However, components of the ANXA1-interacting protein complex remain unclear. Herein, we characterized the interacting complexes of apical membrane (ApANXA1) and cytosolic (cyANXA1) forms of ANXA1 in apical membrane and cytosolic compartments, respectively, of renal epithelial cells under high-calcium condition using proteomic and bioinformatic approaches. After fractionation, the ApANXA1- and CyANXA1-interacting partners were identified by immunoprecipitation followed by nanoLC-ESI-Qq-TOF tandem mass spectrometry (IP-MS/MS). The ANXA1-interacting partners that were common in both apical membrane and cytosolic compartments and those unique in each compartment were then analyzed for their physico-chemical properties (molecular weight, isoelectric point, amino acid contents, instability index, aliphatic index, and grand average of hydropathicity), secondary structure (α-helix, β-turn, random coil, and extended strand), molecular functions, biological processes, reactome pathways and KEGG pathways. The data demonstrated that each set of these interacting proteins exhibited common and unique characteristics and properties. The knowledge from this study may lead to better understanding of the ApANXA1 and CyAXNA1 biochemistry and functions as well as the pathophysiology of CaOx kidney stone formation induced by high-calcium condition.

1. Introduction

Annexin A1 (ANXA1) is a member of the annexins protein family with binding ability to calcium and membrane phospholipids, and plays several roles in cellular processes, including apoptosis, differentiation and proliferation [1]. ANXA1 comprises four repeating motifs with calcium-binding domains [2]. This protein locates mainly in cytoplasm and is also associated with plasma membrane [3]. Several studies have reported anti-inflammatory activity of ANXA1 [4–6], and overexpression of ANXA1 in diabetic mice can relieve diabetes-induced kidney injury [7]. However, its overexpression is associated with several cancers [8–10] and antineutrophil cytoplasmic autoantibody-associated vasculitis [11].

Kidney stone disease has been recognized as a global health problem that leads to significant economic burden [12–14]. Beside the high prevalence and incidence, its high recurrence rate is one of the major problems for this disease [15]. To prevent this disease more effectively and to reduce its economic and other burdens, clearer understanding of its etiologic mechanisms is required. Crystal retention onto renal cell surface is one of the critical processes during initial phase for development of kidney stones, especially calcium oxalate (CaOx), which is the most predominant stone type [16,17]. CaOx crystal retention on the cell surface is affected by several factors, including cellular injury [18–20] and abundance of crystal receptors [21,22].

Hypercalciuria is known as one of the risk factors for CaOx kidney stone disease [23,24]. Several lines of evidence have reported that high urinary calcium concentration is associated with renal cell injury [25–27]. High-calcium condition also increases CaOx crystal retention onto renal epithelial cell surface [28,29] accompanied with the increased expression of surface ANXA1 [28], which is one of the CaOx crystal receptors [30–32]. A previous study using conventional and two-dimensional (2D) Western blot analyses has revealed that a

* Correspondence to: Head of Medical Proteomics Unit, Research Department, Siriraj Hospital, Mahidol University, 6th Floor - SiMR Building, 2 Wanglang Road, Bangkoknoi, Bangkok 10700, Thailand.
E-mail addresses: thongboonkerd@dr.com, vthongbo@yahoo.com (V. Thongboonkerd).

https://doi.org/10.1016/j.csbj.2023.07.037
Received 22 April 2023; Received in revised form 27 July 2023; Accepted 27 July 2023
Available online 29 July 2023

high-molecular-weight form of ANXA1 (at approximately 100 kDa) is expressed on apical membrane, whereas another form with regular molecular weight (at approximately 37 kDa) is present in the cytosol of renal epithelial cells [28]. Additionally, the high-calcium condition increases expression levels of both apical membrane and cytosolic forms of ANXA1 in renal epithelial cells [28]. Moreover, the decreased expression of cell surface ANXA1 by caffeine or estrogen treatment can reduce CaOx crystal retention on renal epithelial cells [31,32].

Similar to other cellular proteins, ANXA1 is expected to interact with many other cellular proteins to govern cellular functions. However, components of the interacting partners of apical membrane ANXA1 (ApANXA1) and cytosolic ANXA1 (CyANXA1) remain unclear. We speculated that the ApANXA1- and CyANXA1-interacting partners might have some different identities, properties and functions. The present study thus aimed to identify and characterize the ApANXA1- and CyANXA1-interacting partners in apical membrane and cytosolic compartments, respectively, of renal epithelial cells under high-calcium condition (to increase expression of ApANXA1 and CyANXA1 [28] and to enhance identification of their interacting complexes). Their interacting complexes were immunoprecipitated and then characterization by tandem mass spectrometry and bioinformatic analyses.

2. Materials & methods

2.1. Cell cultivation and high-calcium treatment

MDCK renal cells (ATCC; Manassas, VA) were maintained in a complete medium containing DMEM (Gibco; Grand Island, NY) supplemented with 60 U/ml penicillin and 60 μg/ml streptomycin (Sigma-Aldrich; Saint Louis, MO) and 10% fetal bovine serum (Gibco) in an incubator with 5% CO_2 at 37 °C. The cells grown in 6-well plate (Corning Costar; Cambridge, MA) served as the non-polarized cells, whereas cell polarization was induced in a Transwell (0.4-μm pore size) (Corning Costar) as previously described [21,33]. The cells were then incubated with 20 mM $CaCl_2$ (Sigma-Aldrich) for 72 h prior to investigations as follows.

2.2. Immunofluorescence staining and laser-scanning confocal microscopy

Immunofluorescence staining and laser-scanning confocal microscopy were performed as described previously [34,35] to confirm that cell polarization was successful. Briefly, non-polarized and polarized MDCK cells were washed twice with ice-cold PBS containing 0.1 mM $CaCl_2$ and 1 mM $MgCl_2$. The cells were then fixed with 4% paraformaldehyde/PBS at 25 °C for 15 min and permeabilized with 0.1% Triton X-100/PBS at 25 °C for 15 min. After blocking followed by three washes with PBS, the cells were incubated with rabbit polyclonal anti-podocalyxin (gp135), rabbit polyclonal anti-calpain-1, or mouse monoclonal anti-Na^+/K^+-ATPase antibody (all were from Santa Cruz Biotechnology; Santa Cruz, CA, and diluted 1:50 in 1% BSA/PBS) at 37 °C for 1 h. After three washes with PBS, the cells were further incubated with corresponding secondary antibody conjugated with Alexa Fluor 488 (Invitrogen; Paisley, UK) (1:2000 in 1% BSA/PBS) mixed with Hoechst's nuclear dye (Invitrogen) (0.1 μg/ml in 1% BSA/PBS) at 37 °C for 1 h. After three washes with PBS, the cells were mounted with 50% glycerol/PBS and examined under a laser-scanning confocal microscope (Eclipse Ti-Clsi4 Laser Unit) (Nikon; Tokyo, Japan) equipped with NIS-Elements AR software (Nikon).

2.3. Fractionation of apical membrane and cytosolic proteins

Peeling method was performed to fractionate and purify apical membrane and cytosolic proteins as described previously [30,36]. After 72-h treatment with 20 mM $CaCl_2$, the polarized cells were washed with ice-cold PBS containing 0.1 mM $CaCl_2$ and 1 mM $MgCl_2$. A filter paper (Whatman; Maidstone, UK) pre-wetted with deionized water was placed on top of the polarized cells for 5 min and then peeled off. Apical membranes adhered and retained under the filter paper were harvested by soaking the filter paper into deionized water followed by gentle scrapping. The remaining cell shafts were then collected as the cytosolic fraction. After drying by lyophilization, proteins in both apical membrane and cytosolic fractions were extracted by using modified RIPA buffer (0.5% Triton X-100, 1 mM EDTA, 150 mM NaCl and 50 mM Tris-HCl; pH 7.4). Concentrations of the recovered proteins were then measured using Bio-Rad Protein Assay (Bio-Rad Laboratories; Hercules, CA). Full details of the peeling procedures as well as the information to convince the efficacy and purity of this method to isolate/purify apical membrane proteins can be found in the previously published article by our group [36].

2.4. Western blot analyses

Equally loaded proteins from each sample (30 μg/sample) were resolved by 12% SDS-PAGE, transferred onto nitrocellulose membrane (Whatman), and incubated with 5% skim milk in PBS for 1 h to avoid non-specific binding. After washing with PBS, the membrane was incubated with rabbit polyclonal anti-podocalyxin (gp135), rabbit polyclonal anti-calpain-1, or mouse monoclonal anti-ANXA1 primary antibody (all were from Santa Cruz Biotechnology and diluted 1:1000 in 1% skim milk/PBS) at 4 °C overnight. After washing with PBS, the membrane was incubated with corresponding secondary antibody conjugated with horseradish peroxidase (Sigma-Aldrich) (1:20,000 in 1% skim milk/PBS) at 25 °C for 1 h and washed with PBS. The membrane was then incubated with SuperSignal West Pico chemiluminescence substrate (Pierce Biotechnology, Inc.; Rockford, IL) to develop immunoreactive bands to be visualized on a radiographic film.

2.5. Affinity purification by immunoprecipitation (IP)

IP was performed as described previously [37,38]. To remove non-specific affinity, proteins in apical membrane and cytosolic fractions were incubated with Protein G Sepharose beads (50% slurry) (GE Healthcare; Uppsala, Sweden) on a tube rotator at 4 °C for 15 min. After 5-min centrifugation at 1,500g, the supernatant was collected and incubated overnight with mouse monoclonal anti-ANXA1 antibody (Santa Cruz Biotechnology) or isotype-control mouse IgG (Santa Cruz Biotechnology) at 4 °C on the rotator. Protein G Sepharose beads (50% slurry) were then added and incubated with the sample on the rotator at 4 °C for 4 h. The beads were collected by 5-min centrifugation at 1,500g and washed with modified RIPA buffer five times. Finally, the protein complexes retained on the beads were eluted using Laemmli's buffer.

2.6. In-solution tryptic digestion and nanoLC-ESI-Qq-TOF MS/MS

In-solution tryptic digestion and nanoLC-ESI-Qq-TOF MS/MS were done as previously described [39,40]. Details are also provided in Supplementary Methods.

2.7. Protein-protein interaction (PPI) network analysis

All sets of the identified proteins, including unique ApANXA1-interacting partners, unique CyANXA1-interacting partners, and common ANXA1-interacting partners (proteins interacted with both ApANXA1 and CyANXA1), were submitted to STRING software (version 11.5) (*www.string-db.org*) to create their PPI networks.

2.8. Analyses of physico-chemical properties

All sets of the identified proteins, including unique ApANXA1-interacting partners, unique CyANXA1-interacting partners, and common ANXA1-interacting partners, were analyzed for various physico-

chemical properties. Molecular weight and isoelectric point (pI) were retrieved from MASCOT search engine (*www.matrixscience.com*). Expasy ProtParam tool (*https://web.expasy.org/protparam*) was employed for computing other properties, such as percentage of amino acid contents, instability index, aliphatic index, and grand average of hydropathicity (GRAVY).

2.9. Secondary structure analysis

All sets of the identified proteins, including unique ApANXA1-interacting partners, unique CyANXA1-interacting partners, and common ANXA1-interacting partners, were analyzed for their secondary structure components using the online Self-Optimized Prediction Method and Alignment (SOPMA) tool (*https://npsa-prabi.ibcp.fr/cgi-bin/npsa_automat.pl?page=/NPSA/npsa_sopma.html*). The default search parameters were used, including number of conformational states = 4 (helix, sheet, turn and coil), window width = 17, and similarity threshold = 8.

2.10. Functional enrichment analysis

All sets of the identified proteins, including unique ApANXA1-interacting partners, unique CyANXA1-interacting partners, and common ANXA1-interacting partners, were analyzed for Gene Ontology (GO) molecular functions using the STRING software (version 11.5) (*www.string-db.org*). Additionally, the ClueGO plugin (version 2.5.9) (*https://apps.cytoscape.org/apps/cluego*) and the Cytoscape software (version 3.9.1) (*https://cytoscape.org*) were used to acquire the GO biological processes, reactome pathways and KEGG pathways of all these sets of these proteins.

2.11. Descriptive statistical analysis

Distribution of each physico-chemical property and percentage of each secondary structure component for the common ANXA1-, unique ApANXA1-, and unique CyANXA1-interacting partners are presented as box plots displaying five important values of each dataset, including minimum, maximum, median, first quartile and third quartile. The box plots were generated by using Microsoft Excel.

3. Results

3.1. Successful polarization of MDCK cells

To confirm that the cell polarization was successful, immunofluorescence staining was performed followed by laser-scanning confocal microscopy. In the non-polarized MDCK cells grown in 6-well plate, expression of markers for apical membrane (podocalyxin/gp135), cytoplasm (calpain-1) and basolateral membrane (Na^+/K^+-ATPase) was diffuse in the cell cytoplasm without membrane organization observed (Fig. 1**A**). In the polarized cells grown in the Transwell, podocalyxin/gp135, calpain-1 and Na^+/K^+-ATPase were specifically localized at apical membrane, cytoplasm and basolateral membrane, respectively (Fig. 1**B**). These data indicate that the cells were successfully polarized in the Transwell system.

3.2. Fractionation of apical membrane and cytosolic proteins and IP of the ApANXA1- and CyANXA1-interacting partners

Apical membrane fraction was isolated by peeling method, whereas the remaining cell shafts served as the cytosolic fraction. To confirm purity of apical membrane and cytosolic proteins in corresponding fractions, Western blot analysis of apical membrane and cytosolic protein markers was performed. The data showed that podocalyxin (or gp135, which is an apical membrane protein marker) and calpain-1 (a cytosolic protein marker) were successfully enriched in apical membrane and cytosolic fractions, respectively, without cross-contaminations between these two fractions (Fig. 2**A and B**). We also confirmed that high-calcium condition (incubated with 20 mM $CaCl_2$) successfully induced the upregulation of ApANXA1 and CyANXA1 as compared with the normal-calcium condition (Figs. 2**C and** 2**D**).

After affinity purification by IP, the efficacy of enrichment of ApANXA1 and CyANXA1 was evaluated. Western blotting revealed that ApANXA1 was successfully pulled down at high molecular sizes (≥

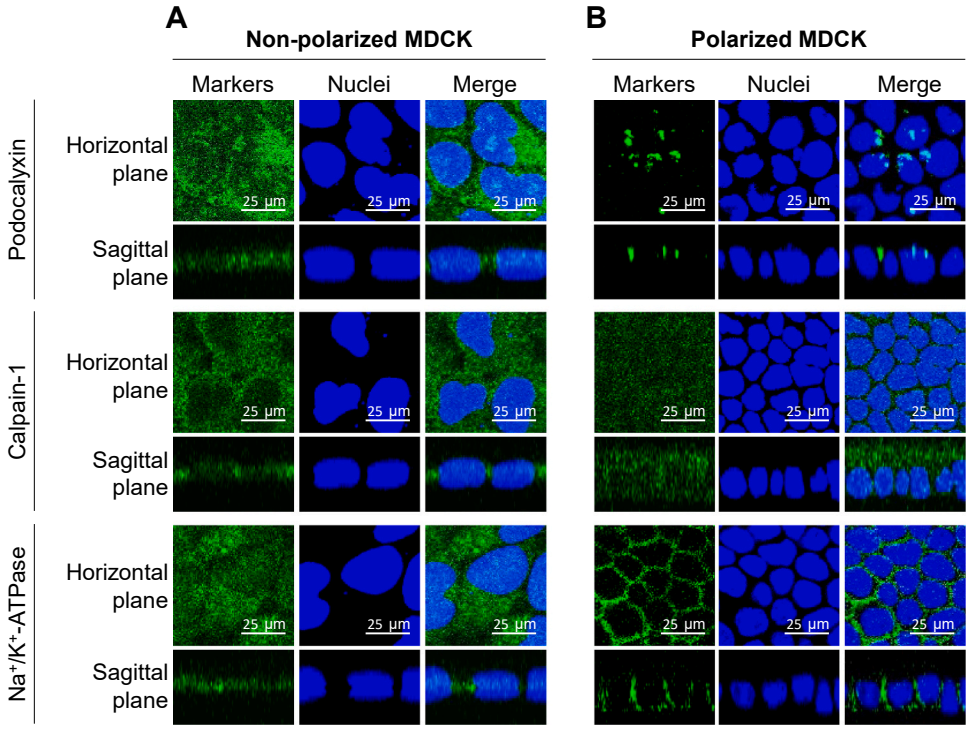

Fig. 1. : Successful polarization of MDCK cells. Immunofluorescence staining and laser-scanning confocal microscopy were performed to confirm that the cell polarization was successful. **(A):** Non-polarized MDCK cells cultured in the 6-well plate. **(B):** Polarized MDCK cells cultured in the Transwell system. All these cells were immuno-stained for podocalyxin (gp135), calpain-1, and Na^+/K^+-ATPase as the protein markers for apical membrane, cytoplasm, and basolateral membrane, respectively.

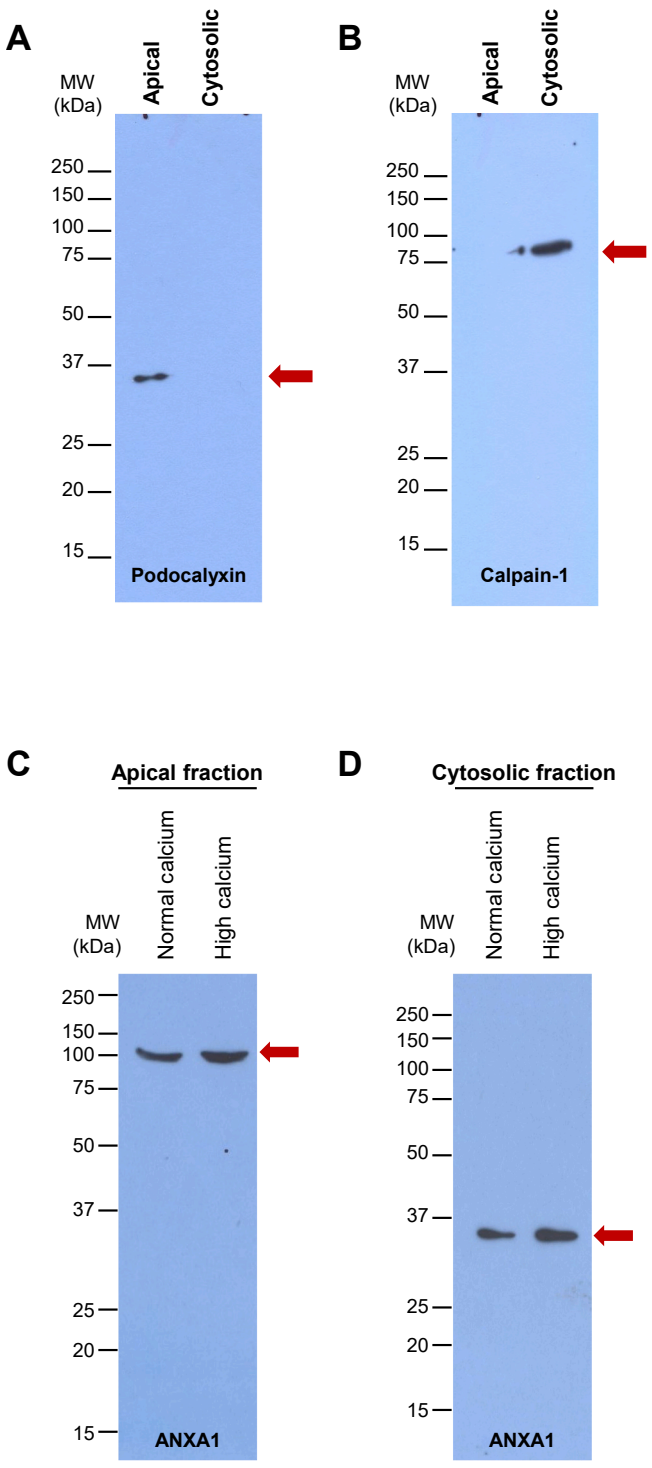

Fig. 2. : Fractionation of apical membrane and cytosolic proteins and upregulation of ApANXA1 and CyANXA1 by high-calcium. (A and B): Western blotting to demonstrate the successful enrichment of markers for apical membrane (podocalyxin or gp135) and cytosolic (calpain-1) proteins in apical membrane and cytosolic fractions, respectively, without cross-contaminations between these two fractions. **(C and D):** Western blotting to confirm that high-calcium condition (incubated with 20 mM $CaCl_2$) successfully induced the upregulation of ApANXA1 and CyANXA1 in the apical membrane and cytosolic fractions, respectively. Note that the ApANXA1 was identified at high molecular sizes (~ 100 kDa) in apical membrane fraction **(C)**, whereas CyANXA1 was identified at regular molecular size (~ 37 kDa) in cytosolic fraction **(D)**. The arrow indicates the target protein.

100 kDa) from apical membrane fraction (Fig. 3**A**), whereas CyANXA1 was successfully pulled down at its regular molecular size (~ 37 kDa) from cytosolic fraction (Fig. 3**B**).

3.3. Identification of ApANXA1- and CyANXA1-interacting partners by nanoLC-ESI-Qq-TOF MS/MS analysis

After IP, the ApANXA1- and CyANXA1-interacting partners were identified by nanoLC-ESI-Qq-TOF MS/MS analysis. Note that proteins, which were found in the isotype-control IP samples (non-specific binders), were excluded from the list. The results revealed a total of 56 ApANXA1-interacting partners (Table 1) and 69 CyANXA1-interacting partners (Table 2). Among these, 37 proteins were identified in both sets and thus defined as the common ANXA1-interacting partners (labelled with ‡), whereas 19 proteins were exclusively identified as the unique ApANXA1-interacting partners (labelled with *) and 32 proteins were exclusively identified as the unique CyANXA1-interacting partners (labelled with #) (Tables 1 and 2**, and** Fig. 4**A**).

3.4. PPI network analysis of the ANXA1-interacting partners

PPI networks of common ANXA1-, unique ApANXA1-, and unique CyANXA1-interacting partners were generated using the STRING tool. The results showed both direct and indirect interactions between ANXA1 and its interacting partners in each set of these proteins. Among the common ANXA1-interacting partners, AHSG, HSP90AA1, ANXA2, CFL1, YWHAX and HSPA8 were directly interacted with of ANXA1 (Fig. 4**B**). For the unique ApANXA1-interacting partners, PRDX1, S100A11, CLU and EZR directly interacted with ANXA1 (Fig. 4**C**). Among the unique CyANXA1-interacting partners, ENO1, PRDX2, HSPA4 and EEF2 had direct interactions with ANXA1 (Fig. 4**D**).

3.5. Analyses of physico-chemical properties of the ANXA1-interacting partners

According to the data retrieved from the MASCOT search engine, range of molecular weights of the unique ApANXA1-interacting partners (11.23–294.06 kDa) was greater than those of the common ANXA1- and unique CyANXA1-interacting partners (9.75–85.12 kDa and 9.25–96.22 kDa, respectively) (Fig. 5**A**). The median for pI of the unique ApANXA1-interacting partners (9.41) was greater than those of the common ANXA1- and unique CyANXA1-interacting partners (7.62 and 7.74, respectively) (Fig. 5**B**). The Expasy ProtParam tool was utilized to analyze other physio-chemical properties of the ANXA1-interacting partners. Content analysis found that non-polar amino acids (Ala, Gly, Ile, Leu, Met, Pro and Val) were the major residues in the ANXA1-interacting partners in all sets with comparable medians of their percentages at 42.50%, 42.00%, and 42.45% for the common ANXA1-, unique ApANXA1-, and unique CyANXA1-interacting partners, respectively (Fig. 5**C**). The medians of positively charged amino acids (Lys and Arg) were greater than those of negatively charged amino acids (Asp and Glu) in all three sets (12.80% vs. 11.50% for common ANXA1-interacting partners, 15.70% vs. 10.80% for unique ApANXA1-interacting partners, and 14.40% vs. 11.40% for unique CyANXA1-interacting partners) (Fig. 5**C**).

The instability indices were at the ranges of 19.64–83.97, 25.20–58.66, and 6.72–73.48 for common ANXA1-, unique ApANXA1-, and unique CyANXA1-interacting partners, respectively (Fig. 5**D**). Classification of stable and unstable proteins based on their instability indices (<40 for the stable proteins) revealed that proportions of the stable proteins in the common ANXA1- and unique ApANXA1-interacting partners were greater than those of the unstable proteins (Fig. 5**E**). By contrast, the unique CyANXA1-interacting partners had greater proportion of the unstable proteins (Fig. 5**E**). Analysis of aliphatic index to indicate thermostability of the proteins found that median of aliphatic indices of the unique ApANXA1-interacting partners

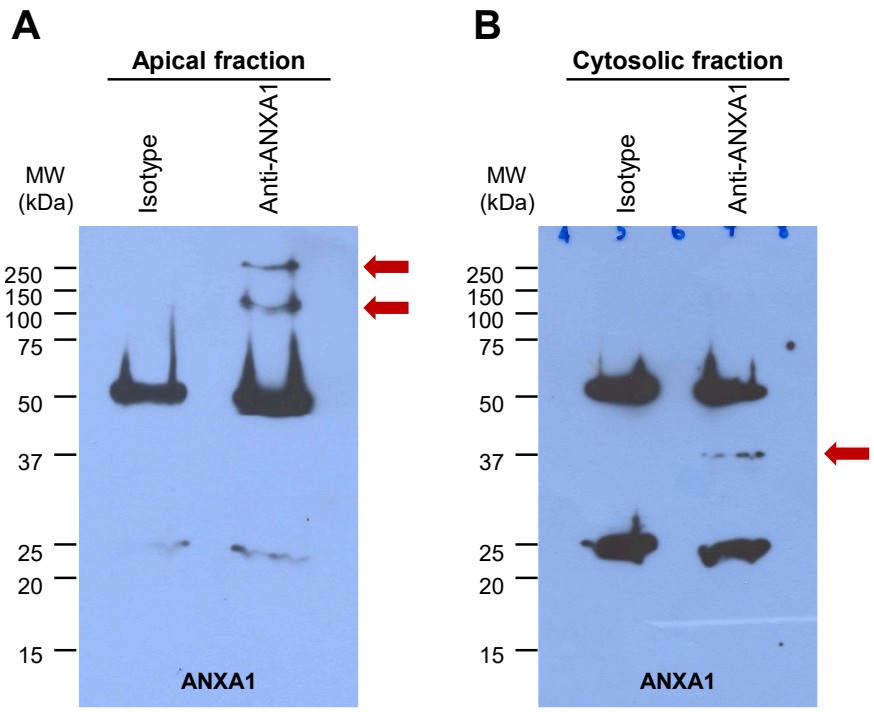

Fig. 3. : IP of ApANXA1- and CyANXA1-interacting partners. (A and B): Western blotting of ANXA1 after affinity purification by IP in apical membrane and cytosolic fractions, respectively. Note that the ApANXA1 was identified at high molecular sizes (≥ 100 kDa) in apical membrane fraction **(A)**, whereas CyANXA1 was identified at regular molecular size (~ 37 kDa) in cytosolic fraction **(B)**. The arrow indicates the ANXA1 band.

was lowest as compared with the common ANXA1- and unique CyANXA1-interacting partners (Fig. 5**F**). Analysis of the grand average of hydropathicity (GRAVY) values revealed that most of the ANXA1-interacting partners in all sets were hydrophilic proteins (with negative GRAVY values) (Fig. 5**G**).

3.6. Secondary structure analysis of the ANXA1-interacting partners

Percentages of four conformational states (α-helix, β-turn, random coil and extended strand/sheet) of the ANXA1-interacting partners were obtained by using the SOPMA tool. The results showed that median percentage of the α-helix was lowest in the unique CyANXA1-interacting partners (36.67%) as compared with the common ANXA1- (41.40%) and unique ApANXA1-interacting partners (42.93%) (Fig. 6**A**). Median percentage of the β-turn was lowest in the unique ApANXA1-interacting partners (5.14%) as compared with the common ANXA1- (7.14%) and unique CyANXA1-interacting partners (6.07%) (Fig. 6**B**). Similarly, median percentage of the extended strand was lowest in the unique ApANXA1-interacting partners (13.28%) as compared with the common ANXA1- (16.44%) and unique CyANXA1-interacting partners (17.38%) (Fig. 6**D**). The median percentage of the random coil was lowest in the common ANXA1-interacting partners (35.10%) as compared with the unique ApANXA1- (38.18%) and unique CyANXA1-interacting partners (39.01%) (Fig. 6**C**).

3.7. Functional enrichment analysis of the ANXA1-interacting partners

GO molecular functions of the ANXA1-interacting partners by using the STRING tool revealed that all sets of these proteins were involved in RNA binding, cadherin binding, and structural constituent of ribosome (Fig. 7). Fifteen GO molecular functions, including small ribosomal subunit rRNA binding, phospholipase A2 inhibitor activity, cell adhesion mediator activity, endopeptidase inhibitor activity, protease binding, unfolded protein binding, MHC class II protein complex binding, enzyme inhibitor activity, ubiquitin protein ligase binding, nucleoside-triphosphatase activity, protein-containing complex binding, enzyme binding, identical protein binding, cell adhesion molecule binding, and structural molecule activity, were observed in the common ANXA1-interacting partners (Fig. 7). Three GO molecular functions, including cadherin binding involved in cell-cell adhesion, calcium-dependent protein binding, and S100 protein binding, were exclusively observed in the unique ApANXA1-interacting partners. However, no unique molecular function was observed for the unique CyANXA1-interacting partners. Most of the molecular functions enriched in the unique CyANXA1-interacting partners overlapped with those enriched in the common ANXA1-interacting partners (Fig. 7).

GO biological process, reactome pathway and KEGG pathway analyses by using Cytoscape-based ClueGO tool revealed that the common ANXA1-interacting partners were mainly involved in metabolic processes and plasminogen activation (Fig. 8**A**), whereas the unique ApANXA1-interacting partners were involved mainly in protein ubiquitination (Fig. 8**B**) and unique CyANXA1-interacting partners were involved mainly in protein localization to mitochondria (Fig. 8**C**).

4. Discussion

ANXA1 is a multifunctional protein involved in various cellular processes and localized in both cytosolic and membrane compartments [1,2]. Usually, proteins work together as a protein complex with their partners. Herein, we characterized the ANXA1-interacting proteins and their roles in both apical membrane and cytosolic compartments of renal epithelial cells under high-calcium condition (to upregulate expression levels of both ApANXA1 and CyANXA1 in renal epithelial cells [28]). Apical membrane and cytosolic compartments were fractionated by the peeling method, which has been established previously [36]. This method is simple and very effective to isolate apical membrane proteins with high purity as confirmed in previous studies [30,36] and herein. The method is based on hydrous affinity and/or ionic interaction between a pre-wetted filter paper and apical membrane of the intact polarized cells [36]. Comparing with other isolation methods, such as

Table 1
Summary of the identified ApANXA1-interacting proteins.

Name	Swiss-Prot ID	Gene symbol	MS/MS score	% Cov	No. of distinct/Total matched peptides	MW (kDa)	pI
‡14–3–3 protein epsilon	P62258	*YWHAE*	203	18.4	5/15	29.33	4.63
‡14–3–3 protein sigma	Q0VC36	*SFN*	49	16.9	5/29	27.95	4.65
‡14–3–3 protein zeta/delta	Q5R651	*YWHAZ*	342	21.2	5/51	27.90	4.73
‡40 S ribosomal protein S14	P13471	*RPS14*	148	15.9	2/11	16.42	10.07
* 40 S ribosomal protein S15a	Q5R938	*RPS15A*	43	5.4	1/2	14.98	10.14
‡40 S ribosomal protein S18	Q3T0R1	*RPS18*	123	13.2	2/11	17.71	10.99
‡40 S ribosomal protein S3	Q0Z8U2	*RPS3*	351	25.5	6/67	26.84	9.68
‡40 S ribosomal protein S4, X isoform	Q76MY1	*RPS4X*	108	14.1	5/48	29.81	10.16
* 40 S ribosomal protein S5	P24050	*RPS5*	43	13.2	3/16	23.04	9.68
‡40 S ribosomal protein SA	Q2L9X0	*RPSA*	95	10.2	3/13	32.96	4.80
‡60 kDa heat shock protein, mitochondrial	Q5NVM5	*HSPD1*	256	15.2	7/28	61.13	5.70
* 60 S ribosomal protein L10-like	Q2TBW8	*RPL10L*	52	11.2	3/10	25.03	10.21
‡60 S ribosomal protein L14	P50914	*RPL14*	82	7.4	2/15	23.53	10.94
* 60 S ribosomal protein L15	Q4R5B2	*RPL15*	65	4.4	1/1	24.25	11.62
* 60 S ribosomal protein L17	Q3T025	*RPL17*	60	8.7	2/6	21.61	10.20
‡60 S ribosomal protein L18a	Q3T003	*RPL18A*	140	18.8	3/17	21.03	10.73
‡60 S ribosomal protein L19	Q3T0W9	*RPL19*	83	13.3	2/8	23.57	11.48
‡60 S ribosomal protein L22	P35268	*RPL22*	86	24.2	3/24	14.84	9.21
* 60 S ribosomal protein L23	Q3T057	*RPL23*	372	7.1	1/27	14.97	10.51
* 60 S ribosomal protein L3	Q29293	*RPL3*	48	3.5	2/9	46.38	10.21
‡60 S ribosomal protein L31	Q1KSC7	*RPL31*	75	26.4	4/37	14.45	10.54
‡60 S ribosomal protein L7	Q4R506	*RPL7*	44	17.4	5/21	29.10	10.70
‡60 S ribosomal protein L7a	Q2TBQ5	*RPL7A*	447	21.4	6/47	30.18	10.61
* 60 S ribosomal protein L8	Q3T0S6	*RPL8*	74	4.3	1/3	28.24	11.03
‡Alpha-1-antiproteinase	P34955	*SERPINA1*	77	9.4	5/30	46.42	6.05
‡Alpha-2-HS-glycoprotein	P12763	*AHSG*	123	11.4	6/39	39.19	5.26
*Annexin A11	P50995	*ANXA11*	149	2.4	1/15	54.70	7.53
‡Annexin A2	A2SW69	*ANXA2*	183	13.0	5/30	38.87	6.92
‡Antithrombin-III	P32262	*SERPINC1*	65	3.9	2/15	52.98	6.44
*Clusterin	Q9XSC5	*CLU*	40	5.4	3/5	52.45	5.49
‡Cofilin-1	Q4R5C0	*CFL1*	223	17.5	4/24	18.79	8.16
‡Elongation factor 1-alpha 1	A2Q0Z0	*EEF1A1*	54	7.8	4/24	50.44	9.10
‡Eukaryotic translation initiation factor 5A-1	Q3T1J1	*EIF5A*	47	5.2	1/8	17.05	5.08
*Ezrin	P15311	*EZR*	41	5.3	4/22	69.48	5.94
‡Fructose-bisphosphate aldolase A	A5A6I5	*ALDOA*	238	19.0	6/53	39.87	8.30
‡Heat shock cognate 71 kDa protein	A2Q0Z1	*HSPA8*	318	12.2	7/58	71.08	5.37
‡Heat shock protein HSP 90-alpha	A5A6K9	*HSP90AA1*	370	15.6	11/101	85.12	4.93
‡Histone H1.3	P16402	*H1–3*	135	18.6	4/22	22.34	11.02
*Histone H2B type 2-E	Q5RCP8	*H2BC21*	53	33.3	5/29	13.92	10.17
‡L-lactate dehydrogenase A chain	P06151	*LDHA*	218	12.0	4/28	36.82	7.62
‡NAD(P)H dehydrogenase [quinone] 1	P05982	*NQO1*	132	3.6	1/5	30.98	8.42
‡Parathymosin	Q9D0J8	*PTMS*	43	10.9	1/7	11.42	4.17
*Peroxiredoxin-1	Q6B4U9	*PRDX1*	76	18.6	4/7	22.34	8.27
‡Platelet factor 4	P02777	*PF4*	498	9.1	1/50	9.75	6.11
*Probable ubiquitin carboxyl-terminal hydrolase FAF-X	P70398	*USP9X*	41	0.3	1/2	294.06	5.57
*Proteasome subunit alpha type-3	Q58DU5	*PSMA3*	39	4.7	1/1	28.62	5.19
‡Proteasome subunit beta type-6	P28072	*PSMB6*	60	8.8	2/6	25.57	4.80
*Protein S100-A11	Q6B345	*S100A11*	43	7.1	1/2	11.23	5.61
‡Pyruvate kinase PKM	P14618	*PKM*	218	14.1	8/58	58.47	7.96
*Serpin A3–2	A2I7M9	*SERPINA3–2*	40	1.9	1/2	46.32	5.67
*T-complex protein 1 subunit delta	Q2T9X2	*CCT4*	42	5.0	4/12	58.68	7.01
*Transcription factor BTF3	P20290	*BTF3*	41	3.4	1/1	22.21	9.41
‡Transgelin-2	P37802	*TAGLN2*	52	14.1	3/12	22.55	8.41
‡Tubulin alpha-3 C chain	P0DPH7	*TUBA3C*	71	6.2	2/19	50.61	4.97
‡Tubulin beta chain	P07437	*TUBB*	402	10.8	5/40	50.10	4.78
‡Tubulin beta-4B chain	Q3MHM5	*TUBB4B*	408	14.2	6/39	50.26	4.79

‡ = Common ANXA1-interacting partners.
* = Unique ApANXA1-interacting partner.
%Cov = Percentage of sequence coverage.

precipitation with $MgCl_2$ or polyethylene glycol followed by sucrose-density gradient centrifugation or differential centrifugation, the peeling method is more effective without significant contaminations from basolateral membrane, cytosolic compartment and intracellular organelles [36]. Moreover, as the peeling method is free of any chemicals during the isolation processes, the physico-chemical properties of apical membrane proteins should be better preserved as compared with the precipitation-based methods, in which chemicals may introduce modifications to the proteins and interfere with PPI [41,42]. In addition, the peeling method has been proven to be very effective for many other studies to isolate and investigate the apical membrane proteins in several various aspects [34,37,43–47].

IP-MS/MS analysis of the ANXA1-interacting partners in apical membrane and cytosolic fractions of renal epithelial cells revealed that number of the ANXA1-interating proteins in cytosolic fraction was greater than that in apical membrane fraction. Some of these identified proteins were present in both fractions. However, there were some unique interacting partners that were exclusively identified in each compartment. We therefore divided the ANXA1-interacting partners into three main sets, including the common ANXA1-interacting partners

Table 2
Summary of the identified CyANXA1-interacting proteins.

Name	Swiss-Prot ID	Gene symbol	MS/MS score	% Cov	No. of distinct/Total matched peptides	MW (kDa)	pI
‡14–3–3 protein epsilon	P62258	*YWHAE*	203	18.4	5/15	29.33	4.63
‡14–3–3 protein sigma	Q0VC36	*SFN*	49	16.9	5/29	27.95	4.65
‡14–3–3 protein zeta/delta	Q5R651	*YWHAZ*	342	21.2	5/51	27.90	4.73
#40 S ribosomal protein S10	Q3T0F4	*RPS10*	127	18.2	3/28	18.89	10.15
‡40 S ribosomal protein S14	P13471	*RPS14*	148	15.9	2/11	16.42	10.07
‡40 S ribosomal protein S18	Q3T0R1	*RPS18*	123	13.2	2/11	17.71	10.99
#40 S ribosomal protein S21	Q9CQR2	*RPS21*	58	12.0	1/10	9.25	8.71
#40 S ribosomal protein S25	Q6Q311	*RPS25*	73	30.4	4/29	13.79	10.12
‡40 S ribosomal protein S3	Q0Z8U2	*RPS3*	351	25.5	6/67	26.84	9.68
‡40 S ribosomal protein S4, X isoform	Q76MY1	*RPS4X*	108	14.1	5/48	29.81	10.16
#40 S ribosomal protein S6	Q4R4K6	*RPS6*	64	10.4	3/19	28.83	10.85
‡40 S ribosomal protein SA	Q2L9X0	*RPSA*	95	10.2	3/13	32.96	4.80
‡60 kDa heat shock protein, mitochondrial	Q5NVM5	*HSPD1*	256	15.2	7/28	61.13	5.70
#60 S ribosomal protein L13	Q9Z313	*RPL13*	183	14.2	3/28	24.44	11.63
#60 S ribosomal protein L13a	Q4R8Z2	*RPL13A*	48	18.2	4/9	23.65	11.03
‡60 S ribosomal protein L14	P50914	*RPL14*	82	7.4	2/15	23.53	10.94
#60 S ribosomal protein L18	P12001	*RPL18*	85	12.8	2/14	21.70	11.79
‡60 S ribosomal protein L18a	Q3T003	*RPL18A*	140	18.8	3/17	21.03	10.73
‡60 S ribosomal protein L19	Q3T0W9	*RPL19*	83	13.3	2/8	23.57	11.48
‡60 S ribosomal protein L22	P35268	*RPL22*	86	24.2	3/24	14.84	9.21
#60 S ribosomal protein L23a	Q24JY1	*RPL23A*	85	13.5	2/9	17.68	10.44
#60 S ribosomal protein L24	Q8BP67	*RPL24*	94	14.0	2/10	17.88	11.26
#60 S ribosomal protein L27a	Q4R723	*RPL27A*	51	10.8	2/3	16.66	11.12
#60 S ribosomal protein L28	Q3T0L7	*RPL28*	83	16.1	2/25	15.74	11.97
‡60 S ribosomal protein L31	Q1KSC7	*RPL31*	75	26.4	4/37	14.45	10.54
#60 S ribosomal protein L34	Q9D1R9	*RPL34*	311	15.4	2/57	13.51	11.47
‡60 S ribosomal protein L7	Q4R506	*RPL7*	44	17.4	5/21	29.10	10.70
‡60 S ribosomal protein L7a	Q2TBQ5	*RPL7A*	447	21.4	6/47	30.18	10.61
‡Alpha-1-antiproteinase	P34955	*SERPINA1*	77	9.4	5/30	46.42	6.05
‡Alpha-2-HS-glycoprotein	P12763	*AHSG*	123	11.4	6/39	39.19	5.26
#Alpha-enolase	P04764	*ENO1*	69	6.5	3/10	47.44	6.16
‡Annexin A2	A2SW69	*ANXA2*	183	13.0	5/30	38.87	6.92
‡Antithrombin-III	P32262	*SERPINC1*	65	3.9	2/15	52.98	6.44
‡Cofilin-1	Q4R5C0	*CFL1*	223	17.5	4/24	18.79	8.16
‡Elongation factor 1-alpha 1	A2Q0Z0	*EEF1A1*	54	7.8	4/24	50.44	9.10
#Elongation factor 2	A0SXL6	*EEF2*	78	6.9	6/36	96.22	6.41
#Endoplasmin	Q4R520	*HSP90B1*	83	4.2	3/14	92.84	4.76
‡Eukaryotic translation initiation factor 5A-1	Q3T1J1	*EIF5A*	47	5.2	1/8	17.05	5.08
‡Fructose-bisphosphate aldolase A	A5A6I5	*ALDOA*	238	19.0	6/53	39.87	8.30
#GTP-binding nuclear protein Ran	Q3T054	*RAN*	41	9.7	2/18	24.58	7.01
#Guanine nucleotide-binding protein subunit beta-2-like 1	Q4R7Y4	*GNB2L1*	129	3.2	1/9	35.51	7.60
#Heat shock 70 kDa protein 4	Q61316	*HSPA4*	105	5.2	5/22	94.87	5.15
‡Heat shock cognate 71 kDa protein	A2Q0Z1	*HSPA8*	318	12.2	7/58	71.08	5.37
‡Heat shock protein HSP 90-alpha	A5A6K9	*HSP90AA1*	370	15.6	11/101	85.12	4.93
#Heat shock protein HSP 90-beta	P11499	*HSP90AB1*	518	20.2	14/110	83.57	4.97
‡Histone H1.3	P16402	*H1–3*	135	18.6	4/22	22.34	11.02
#Histone H2B type 1-K	Q2M2T1	*H2BC12*	66	31.7	5/57	13.87	10.29
#Inosine-5~-monophosphate dehydrogenase 2	Q3SWY3	*IMPDH2*	66	2.3	1/21	56.13	6.87
‡L-lactate dehydrogenase A chain	P06151	*LDHA*	218	12.0	4/28	36.82	7.62
‡NAD(P)H dehydrogenase [quinone] 1	P05982	*NQO1*	132	3.6	1/5	30.98	8.42
‡Parathymosin	Q9D0J8	*PTMS*	43	10.9	1/7	11.42	4.17
#Peptidyl-prolyl cis-trans isomerase FKBP1A	P18203	*FKBP1A*	112	12.0	1/5	11.96	7.88
#Peroxiredoxin-2 (Fragment)	P52552	*PRDX2*	173	21.3	4/53	14.27	4.70
#Plasminogen activator inhibitor 1 RNA-binding protein	Q6AXS5	*SERBP1*	92	5.2	2/18	44.84	8.60
‡Platelet factor 4	P02777	*PF4*	498	9.1	1/50	9.75	6.11
#Poly(rC)-binding protein 1	O19048	*PCBP1*	75	6.2	2/12	37.99	6.66
#Poly(rC)-binding protein 2	Q15366	*PCBP2*	80	6.0	2/14	38.96	6.33
‡Proteasome subunit beta type-6	P28072	*PSMB6*	60	8.8	2/6	25.57	4.80
#Prothymosin alpha	Q5R790	*PTMA*	79	12.7	1/2	12.10	3.69
‡Pyruvate kinase PKM	P14618	*PKM*	218	14.1	8/58	58.47	7.96
#Serotransferrin	Q29443	*TF*	51	11.8	7/33	79.87	6.75
#Serpin A3–5	A2I7N1	*SERPINA3–5*	43	5.1	3/7	46.48	6.48
‡Transgelin-2	P37802	*TAGLN2*	52	14.1	3/12	22.55	8.41
#Transitional endoplasmic reticulum ATPase	Q3ZBT1	*VCP*	142	9.7	6/28	89.96	5.13
#Transthyretin	P12303	*TTR*	93	15.6	2/28	15.88	5.63
‡Tubulin alpha-3 C chain	P0DPH7	*TUBA3C*	71	6.2	2/19	50.61	4.97
‡Tubulin beta chain	P07437	*TUBB*	402	10.8	5/40	50.10	4.78
‡Tubulin beta-4B chain	Q3MHM5	*TUBB4B*	408	14.2	6/39	50.26	4.79
#Ubiquitin-60S ribosomal protein L40	P0C273	*UBA52*	101	24.2	3/18	15.00	9.87

‡ = Common ANXA1-interacting partners.
# = Unique CyANXA1-interacting partner.
%Cov = Percentage of sequence coverage.

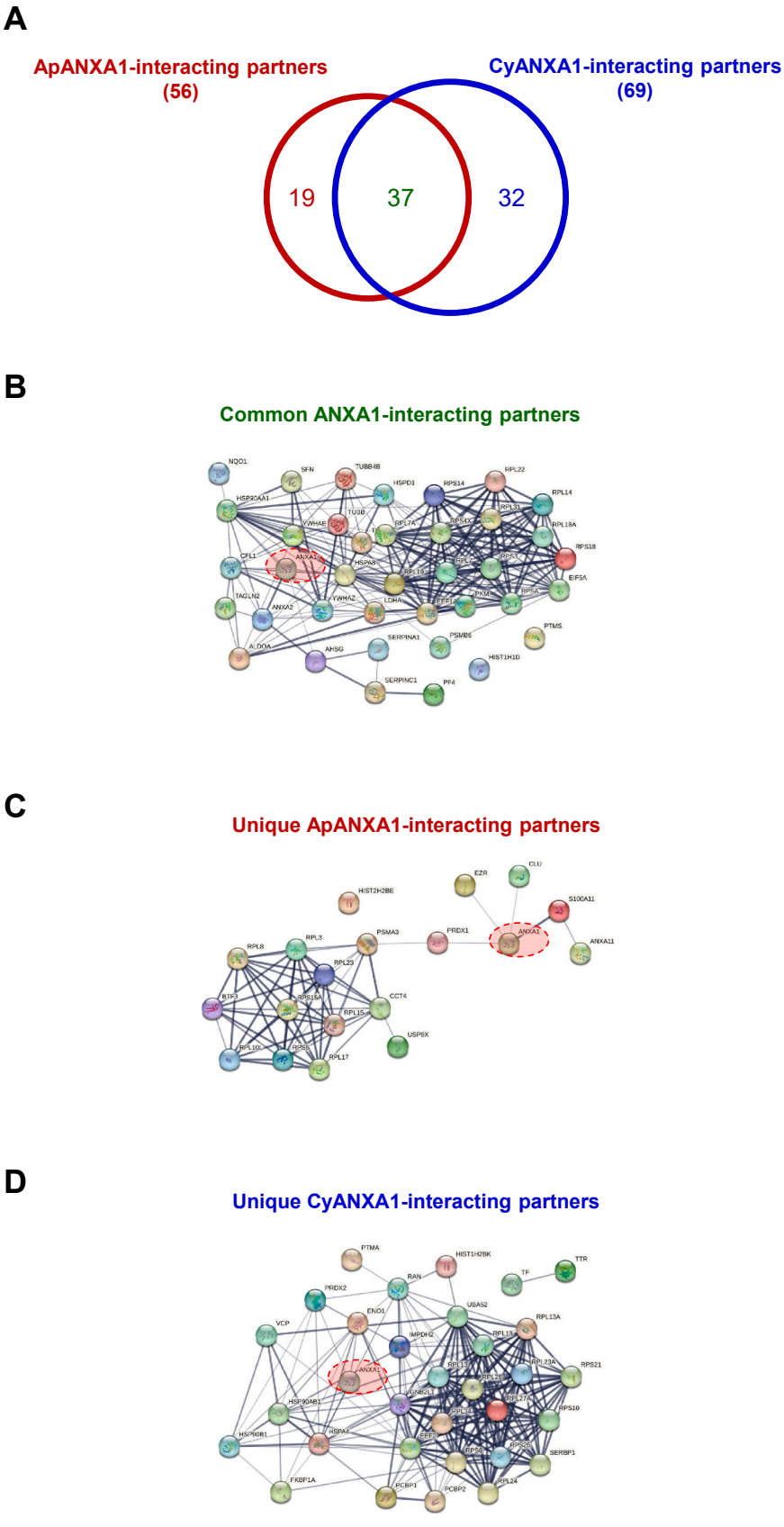

Fig. 4. : MS/MS identification and PPI network analysis of the ANXA1-interacting partners. (A): A Venn diagram summarizing numbers of the unique ApANXA1-interacting partners (exclusively found in apical membrane compartment), common ANXA1-interacting partners (found in both cellular compartments), and unique CyANXA1-interacting partners (exclusively found in cytosolic compartment) (see details in Tables 1 and 2). **(B-D):** PPI network analysis of the common ANXA1-, unique ApANXA1-, and unique CyANXA1-interacting partners, respectively. The thickness of line representing each interaction indicates the confidence level.

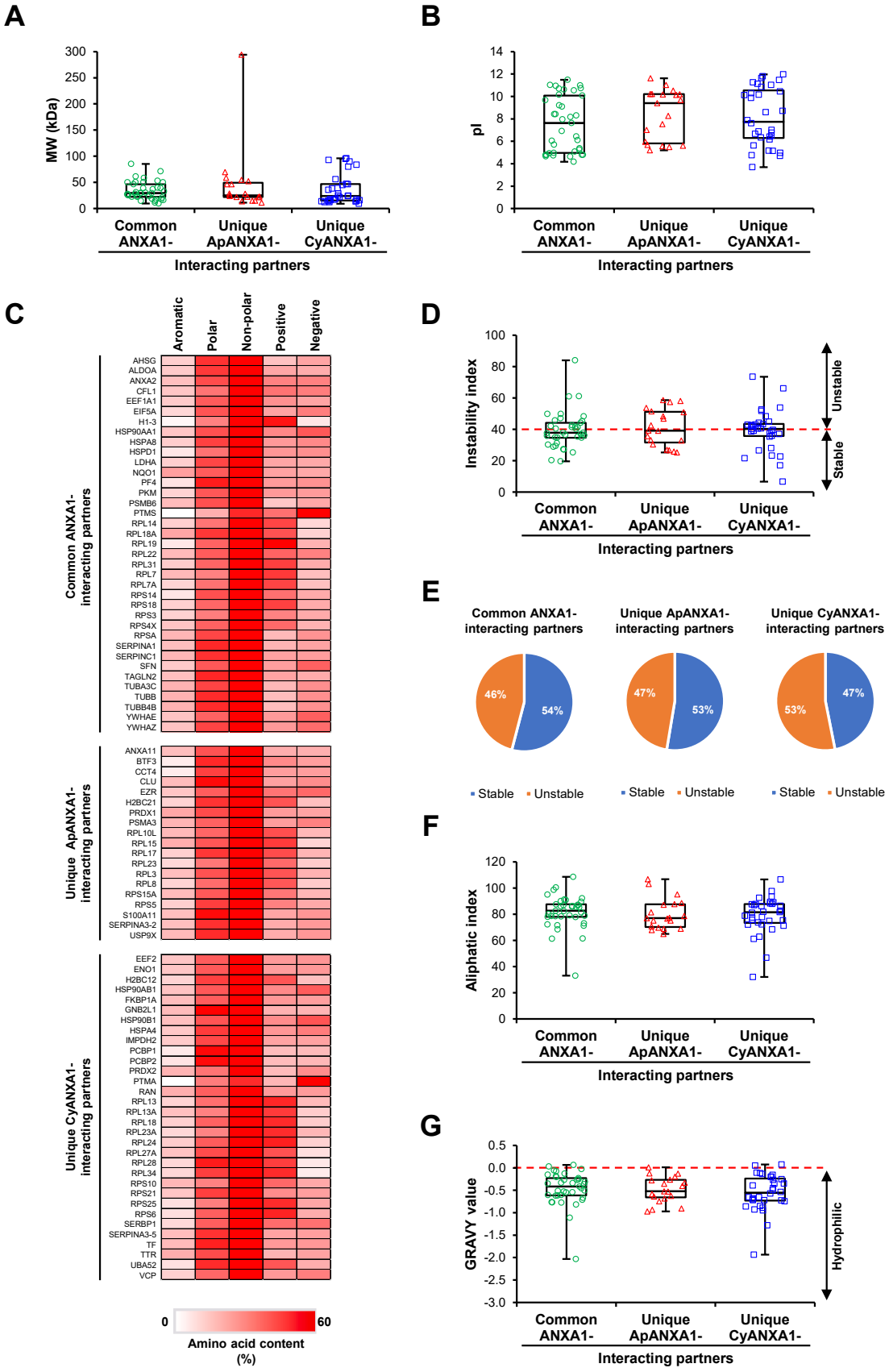

Fig. 5. : Analyses of physico-chemical properties of the ANXA1-interacting partners. (A): Box plot of molecular weight. **(B):** Box plot of pI. **(C):** Heatmap representing percentage of each type of amino acids. **(D):** Box plot of instability index. **(E):** Pie chart representing proportion of stable and unstable proteins based on instability index. **(F):** Box plot of aliphatic index. **(G):** Box plot of GRAVY value.

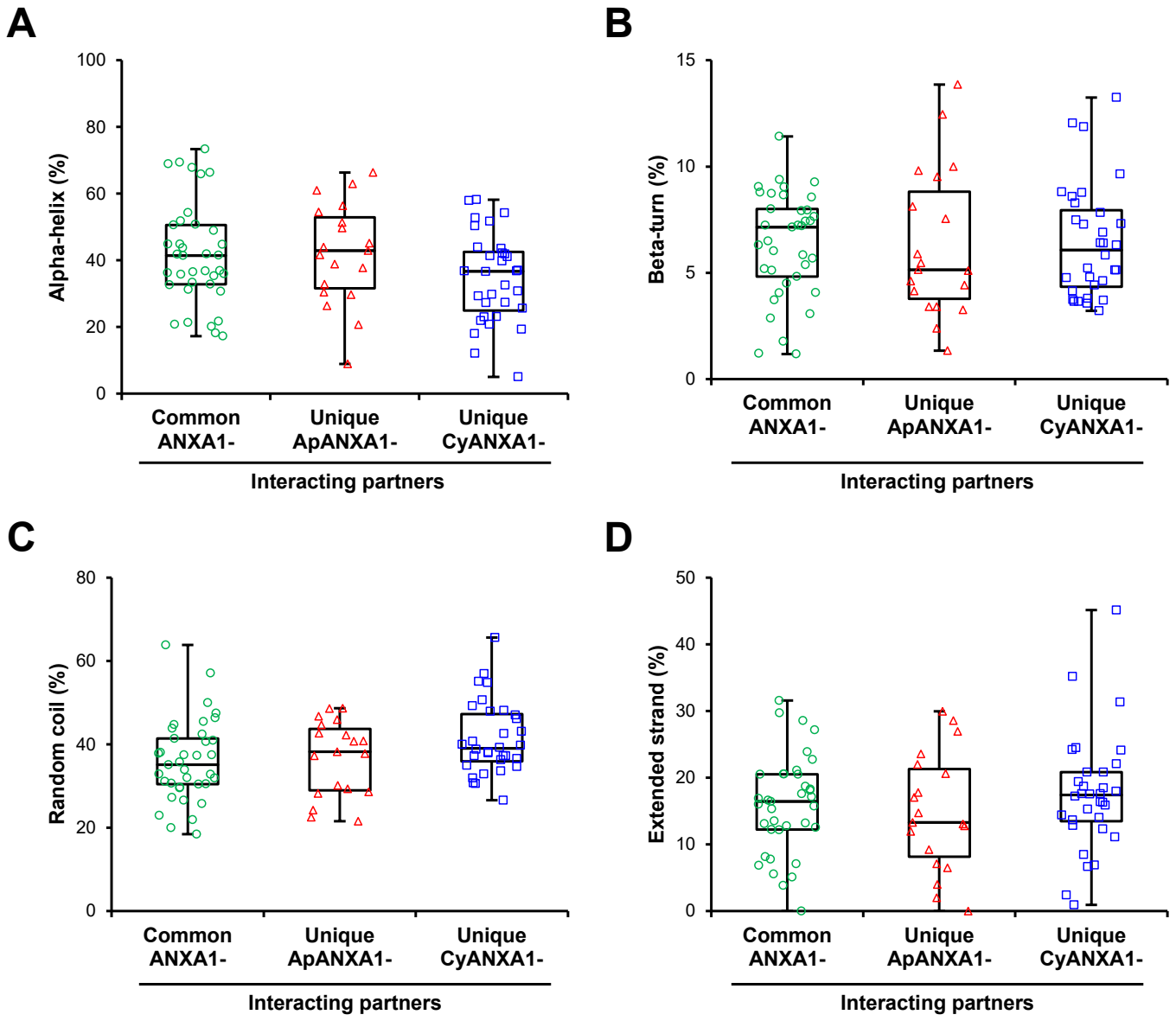

Fig. 6. : Analysis of secondary structure of the ANXA1-interacting partners. (A-D): Box plots of alpha-helices, beta-turns, random coils and extended strands/sheets, respectively.

(37 proteins, which were found in both apical membrane and cytosolic fractions), unique ApANXA1-interacting partners (19 proteins, which were found only in apical membrane fraction), and unique CyANXA1-interacting partners (32 proteins, which were found only in cytosolic fraction).

S100A11 protein was identified as one of the unique ApANXA1-interacting partners and showed direct association with ANXA1 in the PPI network. In concordance, previous studies have reported that calcium facilitates the interaction between ANXA1 and protein S100 family [48,49]. A few other studies have reported the role of S100A11 in calcium-dependent binding of ANXA1 to phospholipids [50,51]. In kidney stone research, S100 proteins have been found in stone matrix [52] with increased levels in urinary exosomes isolated from the stone patients [53]. Herein, GO molecular function enrichment analysis have shown that the unique ApANXA1-binding partners were exclusively involved in calcium-dependent protein binding and S100 protein binding. Moreover, ezrin was identified as another unique ApANXA1-interacting partner, which directly interacted with ANXA1. Ezrin is a membrane-bound protein that belongs to the ERM (ezrin/radixin/moesin) protein family [54]. Ezrin usually serves as a linker between plasma membrane and filamentous actin [54]. Therefore, it plays a major role in regulation of epithelial microvillar structure [55]. Previous studies have suggested that ezrin can bind to several members of S100 proteins [56,57]. S100P proteins interact with ezrin in calcium-dependent manner to regulate actin cytoskeleton-ezrin association [57]. The dissociation of actin cytoskeleton from ezrin has been found in the CaOx-treated renal cells [19].

According to a previous gel-based proteomics study, there are at least two forms of ANXA1 (at approximately 37 and 100 kDa) detected in renal tubular cells [28]. Additionally, levels of these two ANXA1 forms are increased by high-calcium condition [28]. They have been confirmed as ANXA1 by mass spectrometry and Western blotting [28]. Studies on other annexins have found calcium-dependent trimer and multimer, particularly dimer of the trimer of the membrane-bound ANXA5 and ANXB12 [58–61]. Moreover, the calcium-dependent heterotetrametric forms of ANXA1 and ANXA2 together with S100A protein have been found at membrane phospholipid layers [62–65]. Interestingly, ANXA1, S100 protein and ezrin have been characterized as

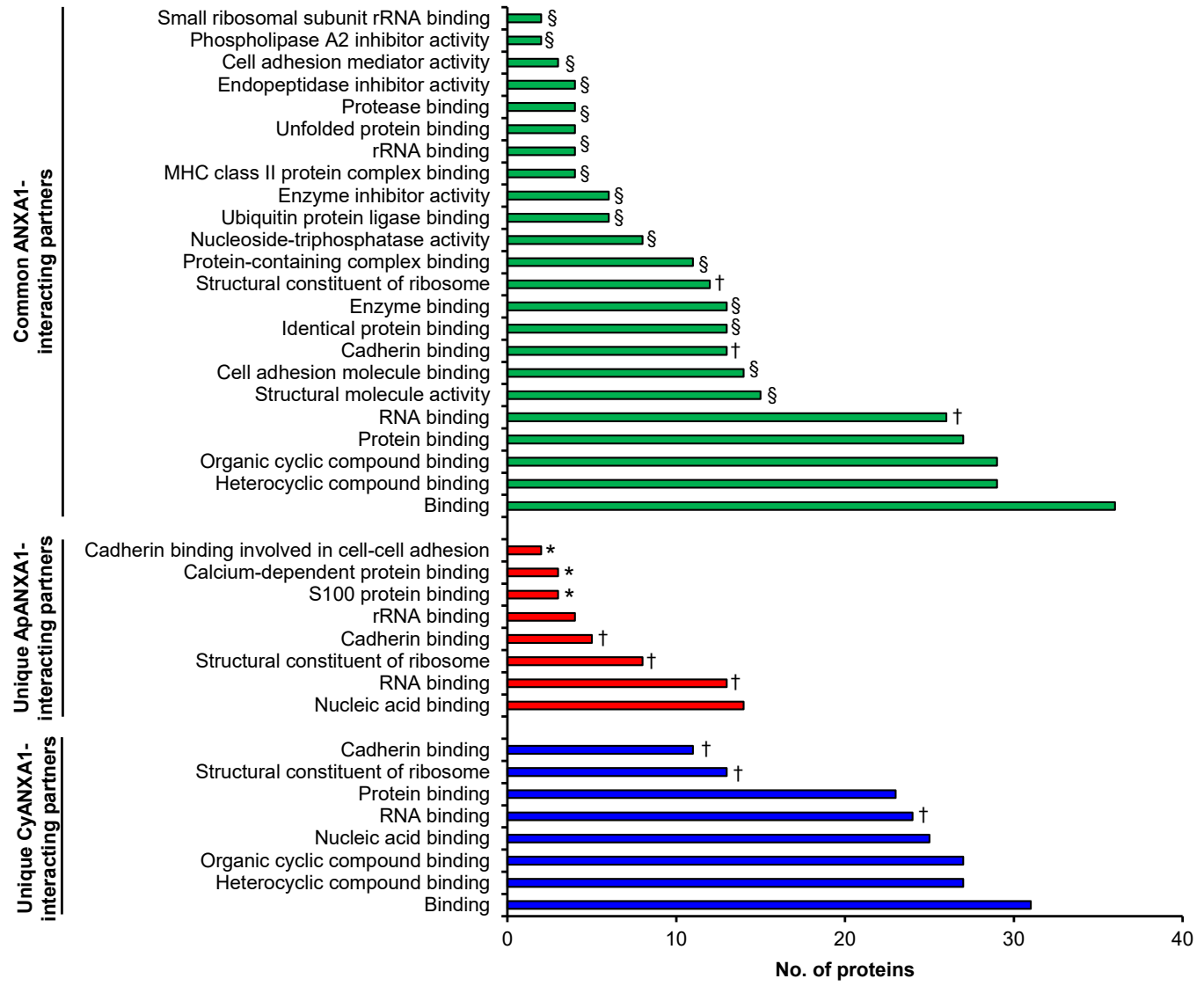

Fig. 7. : GO molecular functions of the ANXA1-interacting partners. † = GO molecular functions enriched in all three sets of the interacting partners, § = GO molecular functions enriched only in the common ANXA1-interacting partners, and * = GO molecular functions enriched only in the unique ApANXA1-interacting partners. Note that there was no unique molecular function observed for the unique CyANXA1-interacting partners.

members of the CaOx crystal receptors [19,28,30,31,34]. Therefore, it is highly possible that the high-molecular-weight form of ANXA1 found at apical membrane fraction (or ApANXA1) is the calcium-induced multimeric form of ANXA1 that specifically serves as the CaOx receptor and may function differently from CyANXA1. Moreover, the unique interactions among these three CaOx crystal receptors on apical membrane would enhance CaOx crystal adhesion and retention on apical membrane of renal tubular cells, leading to kidney stone pathogenesis.

For biological processes, functional enrichment analysis demonstrated that the common ANXA1-interacting partners were involved in several metabolic processes, such as glycolysis, ATP generation from ADP, and ATP biogenesis. In concordance, a previous study has demonstrated that ANXA1 can bind ATP [66]. Additionally, ANXA1 plays roles in regulation of ATP-induced inflammasome activation [67,68]. Multiple lines of additional evidence have also indicated that ANXA1 plays a potential role as an anti-inflammatory protein that is upregulated by several inducers [68,69]. Interestingly, the regulation of inflammation by ANXA1 is accompanied with several proteins localized in both cytosolic and membrane compartments [70].

Analyses of physico-chemical properties showed that molecular weights of the ANXA1-interacting partners were not quite different across the three sets. However, the unique ApAXNA1-interacting partners tended to have higher molecular weights as compared with the others. Analysis of the protein pI demonstrated that pI of the common ANXA1-interacting partners was similar to that of the unique CyANXA1-interacting partners, whereas the unique ApANXA1-interacting partners showed higher pI (more basic). Instability index analysis indicated that majority of the common ANXA1- and unique ApANXA1-interacting partners were relatively more stable proteins, whereas the relatively more unstable proteins were predominantly found in the unique CyANXA1-interacting partners. Additionally, aliphatic index analysis demonstrated that the thermostability of the common ANXA1-interacting partners was comparable to that of the unique CyANXA1 interacting partners, but different from the unique ApANXA1-interacting partners, which showed lower aliphatic index. GRAVY score indicating the hydrophilicity/hydrophobicity of proteins demonstrated that almost all the ANXA1-interacting partners were hydrophilic proteins. This is somewhat surprising that almost all the unique ApANXA1-interacting partners were hydrophilic, because it is well known that membrane proteins are likely to be hydrophobic. However, this may be explained that while ApANXA1 localizes at the membrane, its interacting partners are just associated with it and not necessarily to

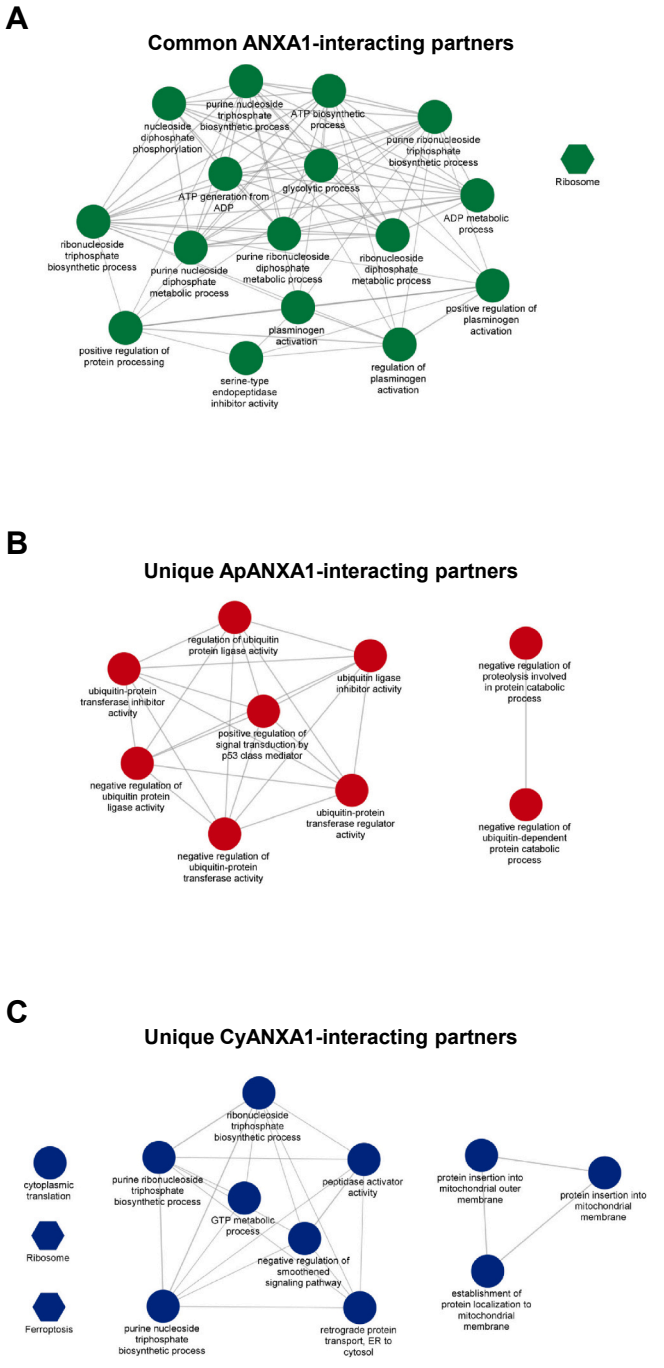

Fig. 8. : GO biological processes, reactome pathways and KEGG pathways of the ANXA1-interacting partners. (A): Common ANXA1-interacting partners. **(B):** Unique ApANXA1-interacting partners. **(C):** Unique CyANXA1-interacting partners.

be the membrane proteins themselves (i.e., serve as the membrane-associated proteins).

Analysis of secondary structure features in each set revealed that most of the secondary conformations found in almost all the ANXA1-interating partners were α-helices. Previous study has suggested that α-helices are less susceptible to mutations than β-strands [71]. Comparing with other sets, the unique CyANXA1-interacting partners had lowest percentage of α-helices but highest percentage of random coils. By contrast, the unique ApANXA1-interacting partners had lowest percentages of β-turns and extended strands.

In conclusion, we report herein identities and characterizations of the interacting partners of ANXA1 in both apical membrane and cytosolic compartments of renal epithelial cells under high-calcium condition. PPI network analysis, analyses of physico-chemical properties, secondary structure prediction, and functional enrichment analysis of these identified proteins have demonstrated that each set of them, including the common ANXA1-interacting partners (found in both cellular compartments), unique ApANXA1-interacting partners (exclusively found in apical membrane compartment), and unique CyANXA1-interacting partners (exclusively found in cytosolic compartment), share some of these characteristics and properties. However, they also have some differences in these characteristics and properties. The knowledge from this study may lead to better understanding of the ApANXA1 and CyAXNA1 biochemistry and functions as well as the pathophysiology of CaOx kidney stone formation induced by high-calcium condition.

CRediT authorship contribution statement

PP and VT designed research; PP and WB performed experiments; PP, WB and VT analyzed data; PP and VT wrote the manuscript; All authors reviewed and approved the manuscript.

Declaration of Competing Interest

The authors declare that they have no known competing financial interests or personal relationships that could have appeared to influence the work reported in this paper.

Acknowledgements

This study was supported by the Thailand Research Fund and Mahidol University (TRG6180011).

Appendix A. Supporting information

Supplementary data associated with this article can be found in the online version at doi:10.1016/j.csbj.2023.07.037.

References

[1] Shao G, Zhou H, Zhang Q, Jin Y, Fu C. Advancements of Annexin A1 in inflammation and tumorigenesis. Onco Targets Ther 2019;12:3245–54. https://doi.org/10.2147/OTT.S202271.
[2] Kelly L, McGrath S, Rodgers L, McCall K, Tulunay Virlan A, Dempsey F, et al. Annexin-A1: the culprit or the solution? Immunology 2022;166(1):2–16. https://doi.org/10.1111/imm.13455.
[3] Mularski A, Sonder SL, Heitmann ASB, Pandey MP, Khandelia H, Nylandsted J, et al. Interplay of membrane crosslinking and curvature induction by annexins. Sci Rep 2022;12(1):22568. https://doi.org/10.1038/s41598-022-26633-w.
[4] Yan Z, Cheng X, Wang T, Hong X, Shao G, Fu C. Therapeutic potential for targeting Annexin A1 in fibrotic diseases. Genes Dis 2022;9(6):1493–505. https://doi.org/10.1016/j.gendis.2022.05.038.
[5] Xu R, Weber MC, Hu X, Neumann PA, Kamaly N. Annexin A1 based inflammation resolving mediators and nanomedicines for inflammatory bowel disease therapy. Semin Immunol 2022;61–64:101664. https://doi.org/10.1016/j.smim.2022.101664.
[6] Gobbetti T, Cooray SN. Annexin A1 and resolution of inflammation: tissue repairing properties and signalling signature. Biol Chem 2016;397(10):981–93. https://doi.org/10.1515/hsz-2016-0200.
[7] Wu L, Liu C, Chang DY, Zhan R, Sun J, Cui SH, et al. Annexin A1 alleviates kidney injury by promoting the resolution of inflammation in diabetic nephropathy. Kidney Int 2021;100(1):107–21. https://doi.org/10.1016/j.kint.2021.02.025.
[8] Zheng L, Li L, Wang B, Zhang S, Fu Z, Cheng A, et al. Annexin A1 affects tumor metastasis through epithelial-mesenchymal transition: a narrative review. Transl Cancer Res 2022;11(12):4416–33. https://doi.org/10.21037/tcr-22-1544.
[9] Cui J, Sachaphibulkij K, Teo WS, Lim HM, Zou L, Ong CN, et al. Annexin-A1 deficiency attenuates stress-induced tumor growth via fatty acid metabolism in mice: an Integrated multiple omics analysis on the stress- microbiome-metabolite-epigenetic-oncology (SMMEO) axis. Theranostics 2022;12(8):3794–817. https://doi.org/10.7150/thno.68611.
[10] Sadashiv R, Bannur BM, Shetty P, Dinesh US, J KV, Deshpande SK, et al. Comparative expression analysis of phospholipid binding protein annexina1 in nephrogenesis and kidney cancer. J Basic Clin Physiol Pharm 2020;31(4):20190179. https://doi.org/10.1515/jbcpp-2019-0179.

[11] Wang RX, Wu L, Chen SF, Li ZY, Zhao MH, Chen M. Renal expression of annexin A1 is associated with the severity of renal injury in antineutrophil cytoplasmic autoantibody-associated vasculitis. Front Med (Lausanne) 2022;9:769813. https://doi.org/10.3389/fmed.2022.769813.

[12] Green BW, Labagnara K, Feiertag N, Gupta K, Donnelly J, Watts KL, et al. Financial toxicity of nephrolithiasis: the first assessment of the economic stresses of kidney stone treatment. Urology 2022;170:46–52. https://doi.org/10.1016/j.urology.2022.08.042.

[13] Thongprayoon C, Krambeck AE, Rule AD. Determining the true burden of kidney stone disease. Nat Rev Nephrol 2020;16(12):736–46. https://doi.org/10.1038/s41581-020-0320-7.

[14] Geraghty RM, Cook P, Walker V, Somani BK. Evaluation of the economic burden of kidney stone disease in the UK: a retrospective cohort study with a mean follow-up of 19 years. BJU Int 2020;125(4):586–94. https://doi.org/10.1111/bju.14991.

[15] Wang K, Ge J, Han W, Wang D, Zhao Y, Shen Y, et al. Risk factors for kidney stone disease recurrence: a comprehensive meta-analysis. BMC Urol 2022;22(1):62. https://doi.org/10.1186/s12894-022-01017-4.

[16] Alexander RT, Fuster DG, Dimke H. Mechanisms underlying calcium nephrolithiasis. Annu Rev Physiol 2022;84:559–83. https://doi.org/10.1146/annurev-physiol-052521-121822.

[17] Wang Z, Zhang Y, Zhang J, Deng Q, Liang H. Recent advances on the mechanisms of kidney stone formation (Review). Int J Mol Med 2021;48(2):149. https://doi.org/10.3892/ijmm.2021.4982.

[18] Khamchun S, Thongboonkerd V. Cell cycle shift from G0/G1 to S and G2/M phases is responsible for increased adhesion of calcium oxalate crystals on repairing renal tubular cells at injured site. Cell Death Discov 2018;4:106. https://doi.org/10.1038/s41420-018-0123-9.

[19] Fong-ngern K, Vinaiphat A, Thongboonkerd V. Microvillar injury in renal tubular epithelial cells induced by calcium oxalate crystal and the protective role of epigallocatechin-3-gallate. FASEB J 2017;31(1):120–31. https://doi.org/10.1096/fj.201600543R.

[20] Wiessner JH, Hasegawa AT, Hung LY, Mandel GS, Mandel NS. Mechanisms of calcium oxalate crystal attachment to injured renal collecting duct cells. Kidney Int 2001;59(2):637–44.

[21] Fong-ngern K, Sueksakit K, Thongboonkerd V. Surface heat shock protein 90 serves as a potential receptor for calcium oxalate crystal on apical membrane of renal tubular epithelial cells. J Biol Inorg Chem 2016;21(4):463–74. https://doi.org/10.1007/s00775-016-1355-x.

[22] Fong-ngern K, Thongboonkerd V. Alpha-enolase on apical surface of renal tubular epithelial cells serves as a calcium oxalate crystal receptor. Sci Rep 2016;6:36103. https://doi.org/10.1038/srep36103.

[23] Coe FL, Worcester EM, Evan AP. Idiopathic hypercalciuria and formation of calcium renal stones. Nat Rev Nephrol 2016;12(9):519–33. https://doi.org/10.1038/nrneph.2016.101.

[24] Guerra A, Ticinesi A, Allegri F, Pinelli S, Aloe R, Meschi T. Idiopathic calcium nephrolithiasis with pure calcium oxalate composition: clinical correlates of the calcium oxalate dihydrate/monohydrate (COD/COM) stone ratio. Urolithiasis 2020;48(3):271–9. https://doi.org/10.1007/s00240-019-01156-8.

[25] Shin S, Ibeh CL, Awuah Boadi E, Choi BE, Roy SK, Bandyopadhyay BC. Hypercalciuria switches Ca(2+) signaling in proximal tubular cells, induces oxidative damage to promote calcium nephrolithiasis. Genes Dis 2022;9(2):531–48. https://doi.org/10.1016/j.gendis.2021.04.006.

[26] Xun Y, Zhou P, Yang Y, Li C, Zhang J, Hu H, et al. Role of Nox4 in high calcium-induced renal oxidative stress damage and crystal deposition. Antioxid Redox Signal 2022;36(1–3):15–38. https://doi.org/10.1089/ars.2020.8159.

[27] Zhao J, Cheng J, Li C, Xu M, Ma C, Qin L, et al. Ethyl pyruvate attenuates CaCl2-induced tubular epithelial cell injury by inhibiting autophagy and inflammatory responses. Kidney Blood Press Res 2018;43(5):1585–95. https://doi.org/10.1159/000494445.

[28] Chutipongtanate S, Fong-ngern K, Peerapen P, Thongboonkerd V. High calcium enhances calcium oxalate crystal binding capacity of renal tubular cells via increased surface annexin A1 but impairs their proliferation and healing. J Proteome Res 2012;11(7):3650–63. https://doi.org/10.1021/pr3000738.

[29] Lieske JC, Farell G, Deganello S. The effect of ions at the surface of calcium oxalate monohydrate crystals on cell-crystal interactions. Urol Res 2004;32(2):117–23.

[30] Fong-ngern K, Peerapen P, Sinchaikul S, Chen ST, Thongboonkerd V. Large-scale identification of calcium oxalate monohydrate crystal-binding proteins on apical membrane of distal renal tubular epithelial cells. J Proteome Res 2011;10(10):4463–77. https://doi.org/10.1021/pr2006878.

[31] Peerapen P, Thongboonkerd V. Caffeine prevents kidney stone formation by translocation of apical surface annexin A1 crystal-binding protein into cytoplasm: In vitro evidence. Sci Rep 2016;6:38536. https://doi.org/10.1038/srep38536.

[32] Peerapen P, Thongboonkerd V. Protective cellular mechanism of estrogen against kidney stone formation: a proteomics approach and functional validation. Proteomics 2019;19(19):e1900095. https://doi.org/10.1002/pmic.201900095.

[33] Manissorn J, Khamchun S, Vinaiphat A, Thongboonkerd V. Alpha-tubulin enhanced renal tubular cell proliferation and tissue repair but reduced cell death and cell-crystal adhesion. Sci Rep 2016;6:28808. https://doi.org/10.1038/srep28808.

[34] Kanlaya R, Thongboonkerd V. Persistent Escherichia coli infection in renal tubular cells enhances calcium oxalate crystal-cell adhesion by inducing ezrin translocation to apical membranes via Rho/ROCK pathway. Cell Mol Life Sci 2022;79(7):381. https://doi.org/10.1007/s00018-022-04414-y.

[35] Kanlaya R, Singhto N, Thongboonkerd V. EGCG decreases binding of calcium oxalate monohydrate crystals onto renal tubular cells via decreased surface expression of alpha-enolase. J Biol Inorg Chem 2016;21(3):339–46. https://doi.org/10.1007/s00775-016-1344-0.

[36] Fong-ngern K, Chiangjong W, Thongboonkerd V. Peeling as a novel, simple, and effective method for isolation of apical membrane from intact polarized epithelial cells. Anal Biochem 2009;395(1):25–32. https://doi.org/10.1016/j.ab.2009.08.007.

[37] Vinaiphat A, Thongboonkerd V. Characterizations of PMCA2-interacting complex and its role as a calcium oxalate crystal-binding protein. Cell Mol Life Sci 2018;75(8):1461–82. https://doi.org/10.1007/s00018-017-2699-2.

[38] Manissorn J, Singhto N, Thongboonkerd V. Characterizations of hsp90-interacting complex in renal cells using tandem affinity purification and its potential role in kidney stone formation. Proteomics 2018;18(24):e1800004. https://doi.org/10.1002/pmic.201800004.

[39] Chanthick C, Thongboonkerd V. Cellular proteome datasets of human endothelial cells under physiologic state and after treatment with caffeine and epigallocatechin-3-gallate. Data Brief 2019;25:104292. https://doi.org/10.1016/j.dib.2019.104292.

[40] Chanthick C, Thongboonkerd V. Comparative proteomics reveals concordant and discordant biochemical effects of caffeine versus epigallocatechin-3-gallate in human endothelial cells. Toxicol Appl Pharm 2019;378:114621. https://doi.org/10.1016/j.taap.2019.114621.

[41] Naowarojna N, Cheng R, Lopez J, Wong C, Qiao L, Liu P. Chemical modifications of proteins and their applications in metalloenzyme studies. Synth Syst Biotechnol 2021;6(1):32–49. https://doi.org/10.1016/j.synbio.2021.01.001.

[42] Sakamoto S, Hamachi I. Recent progress in chemical modification of proteins. Anal Sci 2019;35(1):5–27. https://doi.org/10.2116/analsci.18R003.

[43] Gerl MJ, Sampaio JL, Urban S, Kalvodova L, Verbavatz JM, Binnington B, et al. Quantitative analysis of the lipidomes of the influenza virus envelope and MDCK cell apical membrane. J Cell Biol 2012;196(2):213–21.

[44] Teijeiro JM, Marini PE. Apical membranes prepared by peeling from whole porcine oviducts interact with homologous sperm. Cell Tissue Res 2012;348(1):213–23. https://doi.org/10.1007/s00441-012-1338-3.

[45] Cho KJ, Park JH, Piggott AM, Salim AA, Gorfe AA, Parton RG, et al. Staurosporines disrupt phosphatidylserine trafficking and mislocalize Ras proteins. J Biol Chem 2012;287(52):43573–84. https://doi.org/10.1074/jbc.M112.424457.

[46] Sueksakit K, Thongboonkerd V. Protective effects of finasteride against testosterone-induced calcium oxalate crystallization and crystal-cell adhesion. J Biol Inorg Chem 2019;24(7):973–83. https://doi.org/10.1007/s00775-019-01692-z.

[47] Hellinen L, Sato K, Reinisalo M, Kidron H, Rilla K, Tachikawa M, et al. Quantitative protein expression in the human retinal pigment epithelium: comparison between apical and basolateral plasma membranes with emphasis on transporters. Invest Ophthalmol Vis Sci 2019;60(15):5022–34. https://doi.org/10.1167/iovs.19-27328.

[48] Mailliard WS, Haigler HT, Schlaepfer DD. Calcium-dependent binding of S100C to the N-terminal domain of annexin I. J Biol Chem 1996;271(2):719–25. https://doi.org/10.1074/jbc.271.2.719.

[49] Rety S, Osterloh D, Arie JP, Tabaries S, Seeman J, Russo-Marie F, et al. Structural basis of the Ca(2+)-dependent association between S100C (S100A11) and its target, the N-terminal part of annexin I. Structure 2000;8(2):175–84. https://doi.org/10.1016/s0969-2126(00)00093-9.

[50] Jaiswal JK, Nylandsted J. S100 and annexin proteins identify cell membrane damage as the Achilles heel of metastatic cancer cells. Cell Cycle 2015;14(4):502–9. https://doi.org/10.1080/15384101.2014.995495.

[51] Zhang L, Zhu T, Miao H, Liang B. The calcium binding protein S100A11 and its roles in diseases. Front Cell Dev Biol 2021;9:693262. https://doi.org/10.3389/fcell.2021.693262.

[52] Martelli C, Marzano V, Iavarone F, Huang L, Vincenzoni F, Desiderio C, et al. Characterization of the protein components of matrix stones sheds light on S100-A8 and S100-A9 relevance in the inflammatory pathogenesis of these rare renal calculi. J Urol 2016;196(3):911–8. https://doi.org/10.1016/j.juro.2016.04.064.

[53] Wang Q, Sun Y, Yang Y, Li C, Zhang J, Wang S. Quantitative proteomic analysis of urinary exosomes in kidney stone patients. Transl Androl Urol 2020;9(4):1572–84. https://doi.org/10.21037/tau-20-41.

[54] Senju Y, Tsai FC. A biophysical perspective of the regulatory mechanisms of ezrin/radixin/moesin proteins. Biophys Rev 2022;14(1):199–208. https://doi.org/10.1007/s12551-021-00928-0.

[55] Pelaseyed T, Bretscher A. Regulation of actin-based apical structures on epithelial cells. J Cell Sci 2018;131(20):jcs221853. https://doi.org/10.1242/jcs.221853.

[56] Biri-Kovacs B, Kiss B, Vadaszi H, Gogl G, Palfy G, Torok G, et al. Ezrin interacts with S100A4 via both its N- and C-terminal domains. PLoS One 2017;12(5):e0177489. https://doi.org/10.1371/journal.pone.0177489.

[57] Koltzscher M, Neumann C, Konig S, Gerke V. Ca2+-dependent binding and activation of dormant ezrin by dimeric S100P. Mol Biol Cell 2003;14(6):2372–84. https://doi.org/10.1091/mbc.e02-09-0553.

[58] Oling F, Santos JS, Govorukhina N, Mazeres-Dubut C, Bergsma-Schutter W, Oostergetel G, et al. Structure of membrane-bound annexin A5 trimers: a hybrid cryo-EM - X-ray crystallography study. J Mol Biol 2000;304(4):561–73. https://doi.org/10.1006/jmbi.2000.4183.

[59] Oling F, Bergsma-Schutter W, Brisson A. Trimers, dimers of trimers, and trimers of trimers are common building blocks of annexin a5 two-dimensional crystals. J Struct Biol 2001;133(1):55–63. https://doi.org/10.1006/jsbi.2000.4337.

[60] Tao M, Isas JM, Langen R. Annexin B12 trimer formation is governed by a network of protein-protein and protein-lipid interactions. Sci Rep 2020;10(1):5301. https://doi.org/10.1038/s41598-020-62343-x.

[61] Florentsen CD, Kamp-Sonne A, Moreno-Pescador G, Pezeshkian W, Hakami Zanjani AA, Khandelia H, et al. Annexin A4 trimers are recruited by high membrane curvatures in giant plasma membrane vesicles. Soft Matter 2021;17(2):308–18. https://doi.org/10.1039/d0sm00241k.
[62] Sanchez W, Lindsay S, Li Y. Modeling the Annexin A1-S100A11 heterotetramer: a molecular dynamics investigation of structure and correlated motion. J Biomol Struct Dyn 2023:1–9. https://doi.org/10.1080/07391102.2023.2212804.
[63] Illien F, Finet S, Lambert O, Ayala-Sanmartin J. Different molecular arrangements of the tetrameric annexin 2 modulate the size and dynamics of membrane aggregation. Biochim Biophys Acta 2010;1798(9):1790–6. https://doi.org/10.1016/j.bbamem.2010.05.001.
[64] Gopalakrishnapillai A, Kolb EA, Dhanan P, Mason RW, Napper A, Barwe SP. Disruption of annexin ii /p11 interaction suppresses leukemia cell binding, homing and engraftment, and sensitizes the leukemia cells to chemotherapy. PLoS One 2015;10(10):e0140564. https://doi.org/10.1371/journal.pone.0140564.
[65] Hu W, Bhattacharya S, Hong T, Wong P, Li L, Vaidehi N, et al. Structural characterization of a dimeric complex between the short cytoplasmic domain of CEACAM1 and the pseudo tetramer of S100A10-Annexin A2 using NMR and molecular dynamics. Biochim Biophys Acta Biomembr 2021;1863(1):183451. https://doi.org/10.1016/j.bbamem.2020.183451.
[66] Han HY, Lee YH, Oh JY, Na DS, Lee BJ. NMR analyses of the interactions of human annexin I with ATP, Ca2+, and Mg2+. FEBS Lett 1998;425(3):523–7. https://doi.org/10.1016/s0014-5793(98)00301-9.
[67] Galvao I, de Carvalho RVH, Vago JP, Silva ALN, Carvalho TG, Antunes MM, et al. The role of annexin A1 in the modulation of the NLRP3 inflammasome. Immunology 2020;160(1):78–89. https://doi.org/10.1111/imm.13184.
[68] Wu C, Qiu T, Yuan W, Shi Y, Yao X, Jiang L, et al. Annexin A1 inhibition facilitates NLRP3 inflammasome activation in arsenic-induced insulin resistance in rat liver. Environ Toxicol Pharm 2022;96:103981. https://doi.org/10.1016/j.etap.2022.103981.
[69] Zhang Z, Ma Q, Velagapudi R, Barclay WE, Rodriguiz RM, Wetsel WC, et al. Annexin-A1 tripeptide attenuates surgery-induced neuroinflammation and memory deficits through regulation the NLRP3 inflammasome. Front Immunol 2022;13:856254. https://doi.org/10.3389/fimmu.2022.856254.
[70] Han PF, Che XD, Li HZ, Gao YY, Wei XC, Li PC. Annexin A1 involved in the regulation of inflammation and cell signaling pathways. Chin J Trauma 2020;23(2):96–101. https://doi.org/10.1016/j.cjtee.2020.02.002.
[71] Abrusan G, Marsh JA. Alpha helices are more robust to mutations than beta strands. PLoS Comput Biol 2016;12(12):e1005242. https://doi.org/10.1371/journal.pcbi.1005242.